Nuclear Engineering and Technology 49 (2017) 1748–1751

Contents lists available at ScienceDirect

Nuclear Engineering and Technology

journal homepage: www.elsevier.com/locate/net

Original Article

Hydrogen's influence on reduced activation ferritic/martensitic steels' elastic properties: density functional theory combined with experiment

Sinan Zhu, Chi Zhang*, Zhigang Yang, Chenchong Wang

Key Laboratory of Advanced Materials of Ministry of Education, School of Materials Science and Engineering, Tsinghua University, No. 1 Qinghua Yuan, North Zhongguancun Street, Beijing 100084, China

ARTICLE INFO

Article history:
Received 1 June 2017
Received in revised form
31 July 2017
Accepted 22 August 2017
Available online 16 October 2017

Keywords:
Density Functional Theory
Experiment
Elastic Properties
Hydrogen
RAFM Steels

ABSTRACT

Reduced activation ferritic/martensitic (RAFM) steels are widely applied as structural materials in the nuclear industry. To investigate hydrogen's effect on RAFM steels' elastic properties and the mechanism of that effect, a procedure of first principles simulation combined with experiment was designed. Density functional theory models were established to simulate RAFM steels' elastic status before and after hydrogen's insertion. Also, experiment was designed to measure the Young's modulus of RAFM steel samples with and without hydrogen charging. Both simulation and experiment showed that the solubility of hydrogen in RAFM steels would decrease the Young's modulus. The effect of hydrogen on RAFM steels' Young's modulus was more significant in water-quenched steels than it was in tempering steels. This indicated that defects inside martensite, considered to be hydrogen traps, could decrease the cohesive energy of the matrix and lead to a decrease of the Young's modulus after hydrogen insertion.

1. Introduction

Reduced activation ferritic/martensitic (RAFM) steels are widely applied as structural materials in fusion reactors, owing to their excellent performance in withstanding heat flux and neutron beam [1–3]. Considering the service environment, hydrogen tends to exert some influence on RAFM steels' properties, especially the mechanical properties. Indeed, hydrogen's effect on steels has been investigated widely for a long time [4,5].

However, the mechanism of hydrogen's influence on steel properties has remained unclear so far. Various conclusions have been presented with respect to different steel compositions, heat treatment processes, experiment methods, and simulation procedures [6–9]. Usui and Shigeru's experimental work [6] based on Fe–Cr–Mn austenite indicated that hydrogen charging increased the Young's modulus. However, Ortiz and Ovejero-Garcia's experimental results [7] on AISI 1005 and 1070 steels drew an opposite conclusion: hydrogen decreased the Young's modulus. D. Psiachos et al.'s ab initio study [8] manifested that interstitial hydrogen decreased the elastic constants of α-iron. As mentioned, the effect of hydrogen on steel elastic properties significantly varied for different steels. With respect to hydrogen embrittlement, very few investigations have focused on contemporary structural materials of the nuclear industry. Therefore, the effect of hydrogen on RAFM steels and the mechanism of that effect are still unclear, which will probably be a limitation in fusion reactor development. Meanwhile, simulation and experiment on hydrogen embrittlement have usually been operated in isolation and have lacked a necessary combined approach.

In this work, we focused on hydrogen's influence on RAFM steels' elastic properties, adopting both density functional theory (DFT) simulation and experiment. The effect of hydrogen on RAFM steels' elastic modulus was studied, and the mechanism of that effect was analyzed by comparison of simulation and experimental results.

2. Material and methods

The main composition of our RAFM is shown in Table 1. Based on the material, DFT computational models and corresponding experiments were designed.

Two models were built as shown in Fig. 1. Model A was a 2 × 2 × 2 supercell, of which the unit cell was a body-centered cubic (BCC) Fe cell. The Fe atom at the center position was replaced

* *Corresponding author.*
E-mail address: chizhang@tsinghua.edu.cn (C. Zhang).

https://doi.org/10.1016/j.net.2017.08.021

Table 1
Chemical compositions (wt%) of the RAFM.

Elements	Cr	W	Mn	V	C	Ta	N	P	S	Fe
Proportion	8.6	1.5	0.55	0.29	0.102	0.09	0.024	0.005	0.001	Bal

RAFM, reduced activation ferritic/martensitic.

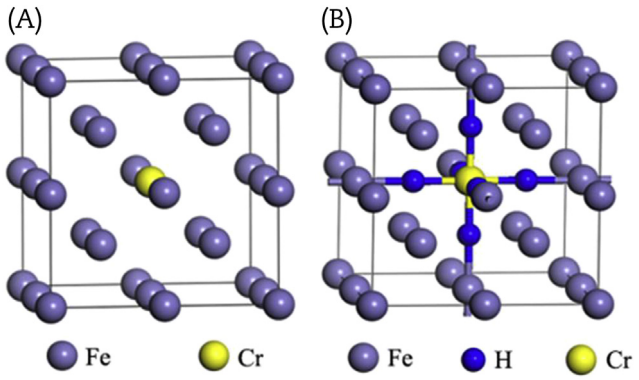

Fig. 1. DFT computational models. (A) Fe–Cr alloy model. (B) Fe–Cr alloy model inserted with hydrogen atoms.

by a Cr atom. This model was used to represent the original matrix of RAFM steels without hydrogen. Model B had hydrogen atoms inserted at six neighbor octahedral interstitial sites away from the center position, based on model A. Considering that the mass concentration of hydrogen in steel materials was less than 10^{-6} ppm [10,11], the atom occupancy of each hydrogen position in model B was set to 1.2×10^{-4}.

In the present work, first principles calculations were performed using DFT, based on the Cambridge Serial Total Energy Package code. The generalized gradient approximation with the Perdew and Wang functional (GGA-PW91) was adopted for the exchange-correlation. The $2 \times 2 \times 2$ BCC supercells in models A and B were used, and the energy was set to cut off at 400 eV; a $4 \times 4 \times 4$ **k** point mesh, derived using the Monkhorst-Pack scheme, was adopted to sample the Brillouin zone. During the geometry optimization, we chose convergence tolerance criteria of 0.05 eV/Å for force, 2×10^{-5} eV/atom for energy, 0.1 GPa for stress, and 0.002 Å for displacement [8,12–17].

After convergence, we adopted the stress–strain method on the basis of the optimized structure to calculate the elastic constants [17], using GGA-PW91. The convergence tolerance criteria were set at 0.01 eV/Å for force, 4×10^{-6} eV/atom for energy, and 4×10^{-4} Å for displacement. We chose the maximum strain amplitude of 0.003 in this work.

The steels for experiment were produced as cylindrical samples with 10 mm diameter and 20 mm height. These samples were first quenched with 20°C water at 990°C and then divided into two groups of A and B. Group A was laid aside at room temperature, while group B was kept at 400°C for 4 hour (tempering treatment), so as to prepare samples with different structures. After the thermal treatment, all the samples were gently polished, and a pair of samples in each group was picked out for subsequent experiments.

An electrochemical method was chosen to charge hydrogen into the RAFM steel samples, as shown in Fig. 2. In an electrolytic tank, containing 0.5 mol/L NaOH solution, the steel samples and platinum sheets were linked to cathodes and anodes of a constant current source, respectively. The current density was set at 0.3 A/cm^2; the hydrogen charging processing lasted for 4 hour each time. For each pair of samples, one was charged with hydrogen, and

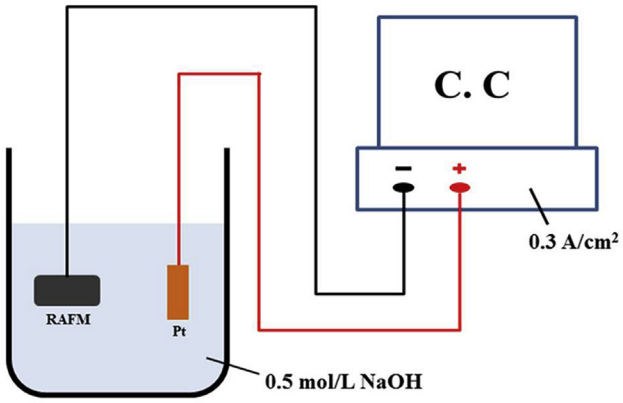

Fig. 2. Hydrogen-charging device. RAFM, reduced activation ferritic/martensitic.

the other was not. The compression experiment was implemented within 1 hour of the hydrogen charging.

The compression experiment, adopting the WDW-100/E electronic universal testing machine, was used to acquire the force-displacement relation data. Based on the data, we were able to draw the stress–stain curves and observe the elastic stage of the curves. The difference in slope of the two curves in the elastic stage, representing samples with and without hydrogen charging, was found to reflect the elastic modulus variation tendency after hydrogen entry.

3. Results

3.1. Simulation results

Based on the simulation results of Cambridge Serial Total Energy Package (C_{11}, C_{12}, C_{44}), the elastic properties of models A and B, including bulk modulus B (GPa), shear modulus G (GPa), and the very important Young's modulus E (GPa), were calculated using the following equations [17,18]:

$$B = \frac{C_{11} + 2C_{12}}{3} \tag{1}$$

$$G = \frac{C_{11} - C_{12} + 3C_{44}}{5} \tag{2}$$

$$E = \frac{9BG}{3B + G} \tag{3}$$

According to Table 2, compared with the case of model A, both bulk modulus (B) and shear modulus (G) of model B decreased. The calculated Young's modulus (E) also decreased.

3.2. Experimental results

In Fig. 3, the red lines represent the samples without hydrogen charging, while the black dashed lines represent the samples

Table 2
The calculated bulk modulus (B), shear modulus (G), Young's modulus (E) for model A and B.

Model	B	G	E
A	292.86	64.97	181.49
B	243.33	51.98	145.57

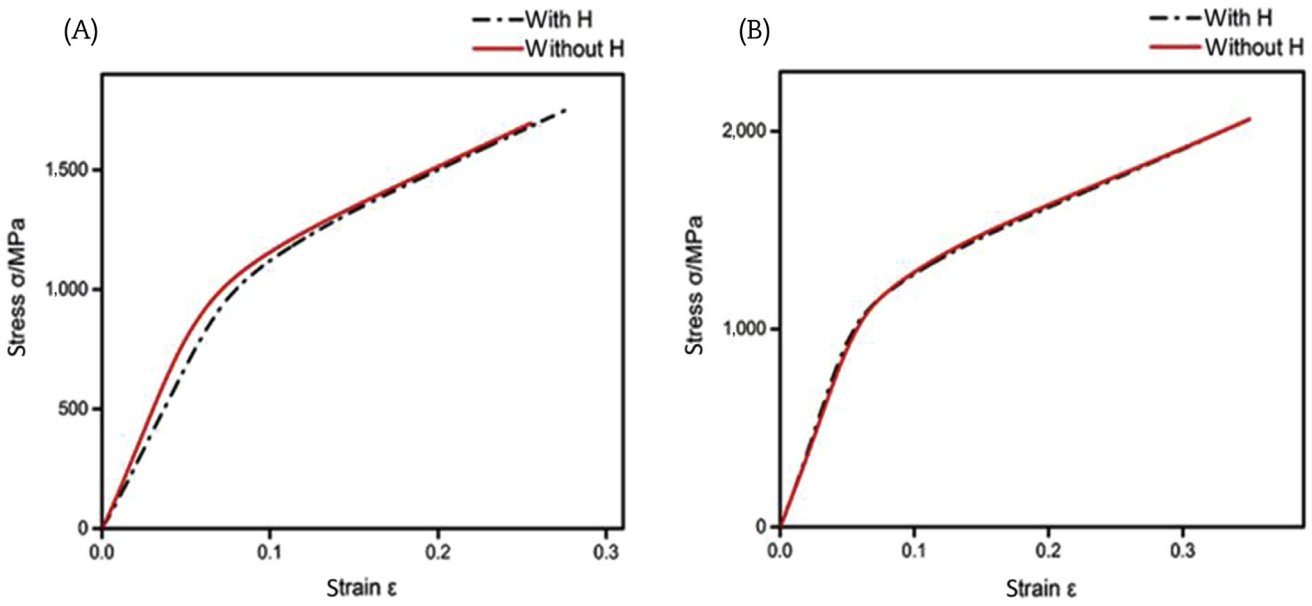

Fig. 3. The curves acquired from the force-displacement relation data. (A)The stress–strain curve of sample pair selected from the group A. (B) The stress–strain curve of sample pair selected from the group B.

charged with hydrogen. The slope of the linear stage represents the Young's modulus. In Fig. 3A, comparing the linear stage of red and black lines, the hydrogen charging sample's Young's modulus was 3.9 GPa less than that of the sample without hydrogen charging. In Fig. 3B, the red line nearly overlaps with the black dashed line, and the calculated Young's modulus' difference between hydrogen charged sample and the no-hydrogen sample was less than 0.1 GPa.

4. Discussion

In DFT simulation, the bulk modulus, usually considered to be a standard of deformation resistance capacity [19,20], decreased from model A to model B. The calculated Young's modulus also decreased. The only difference between models A and B was H atom insertion, indicating that hydrogen can cause a decrease of elastic modulus in the Fe–Cr system, which was similar to Psiachos et al.'s ab initio simulation results [8].

The experimental results also provided important evidence. The main structure of water-quenched steels was martensite, of which the substructure contained a high density of defects, such as dislocations and holes [21–23]. These defects, considered to be hydrogen traps, provided positions for hydrogen atoms to gather, increasing the hydrogen concentration in martensite. The samples from group A, which were water-quenched RAFM steels, were susceptible to hydrogen because the defects captured enough hydrogen to exert an effect on the elastic modulus. In contrast, the samples from group B were not susceptible to hydrogen because of the decline of the defect density after the tempering treatment [24], which reduced the hydrogen concentration remarkably, such that its effect on the Young's modulus became tiny. In general, hydrogen tends to influence the strength of steels. Nevertheless, a compression experiment is not as susceptible as a tensile test to the change of strength; therefore, in our experiment, we focused only on the elastic modulus, which is easier to detect. In summary, the experimental results indicated that hydrogen would decrease RAFM steels' Young's modulus, which was similar to Ortiz and Ovejero-Garcia's experimental results [7] on AISI 1005 and 1070 steels.

The experimental results were basically consistent with the DFT simulation results. The simulation showed that RAFM steels' Young's modulus decreased with hydrogen atom insertion, while the experiment showed the same tendency, and showed the mechanism of hydrogen insertion: defects inside martensite capture hydrogen. Ortiz and Ovejero-Garcia's work [7] provided a similar explanation, showing that lattice defects promote hydrogen gathering, reducing Young's modulus. Meanwhile, their experimental materials also had a martensitic structure. The determinant factor of the metal elastic modulus is the cohesive energy [25,26]. Psiachos et al.'s ab initio study indicated that the dominant reason for elastic constant decrease was the increase of volume per atom, owing to hydrogen insertion [8]. We agree with this point because the increase of volume is accompanied by an extension of the distance between atoms, decreasing the average cohesive energy. From the DFT simulation combined with the experiment, we can confidently state that the hydrogen gathering in martensite structure defects leads to a decrease of the cohesive energy, exerting an influence on RAFM steels' elastic properties.

Different results by Usui and Shigeru [6] on Fe–Cr–Mn austenitic steel might be explained by a difference in structure: austenitic steel, with low density of defects, captured less hydrogen than water-quenched martensite, and therefore, the dominant reason for the Young's modulus' change might be the redistribution of inner stress caused by hydrogen insertion, rather than the increase of volume. Apart from this, the resonant method adopted by the former study [6,11] measured the Young's modulus more precisely than our compression machine, being able to detect the effect of minute quantities of hydrogen. These effects, which might have been ignored in the compression experiment, were recorded by more precise methods, and this resulted in the different conclusion. Also, the DFT models we established were imperfect; the proportion of Fe to Cr was not accurately consistent with reality, and many other compositions were omitted. The simplified supercell, lacking consideration of defects, could not be used to simulate hydrogen trapping in reality, which accounted for the obvious numerical difference between the simulation and the experimental results.

To investigate hydrogen's influence on RAFM steels' elastic properties and the mechanism of that influence, we managed to combine DFT simulation and experiment:

1. DFT simulation results showed that hydrogen solubility will decrease the Young's modulus of the Fe–Cr system.
2. The experiment showed that hydrogen charging remarkably decreased water-quenched RAFM steels' Young's modulus; nevertheless, this phenomenon became inconspicuous for samples undergoing 4-hour 400°C tempering treatment.
3. Comparing the simulation and the experimental results, hydrogen trapping by defects inside martensite, which could decrease the cohesive energy, is probably the intrinsic reason for the decrease of RAFM steels' Young's modulus.

Conflicts of interest

The authors have no conflicts of interest.

References

[1] W. Wang, S.J. Liu, G. Xu, B.R. Zhang, Q.Y. Huang, Effect of thermal aging on microstructure and mechanical properties of China low-activation martensitic steel at 550°C, Nucl. Eng. Technol. 48 (2016) 518–524.

[2] C.C. Wang, C. Zhang, Z.G. Yang, J.J. Zhao, Multiscale simulation of yield strength in reduced-activation ferritic/martensitic steel, Nucl. Eng. Technol. 49 (2017) 569–575.

[3] Z.X. Xia, C. Zhang, H. Lan, Z.Q. Liu, Z.G. Yang, Effect of magnetic field on interfacial energy and precipitation behavior of carbides in reduced activation steels, Mater. Lett. 65 (2011) 937–939.

[4] V.V. Panasyuk, Decohesive concept of the interaction of hydrogen with metals, Mater. Sci. 50 (2014) 161–169.

[5] B.G. Mytsyk, Ya.L. Ivanytskyi, A.I. Balitskii, Ya.P. Kost', O.M. Sakharuk, Study of hydrogen influence on 1020 steel by low deformation method, Mater. Lett. 184 (2016) 328–331.

[6] Makoto Usui, Shigeru Asano, Effect of hydrogen on internal friction and Young's modulus of Fe-Cr-Mn austenitic stainless steel, Scr. Mater. 34 (1996) 1691–1696.

[7] M. Ortiz, J. Ovejero-Garcia, Effect of hydrogen on Young's modulus of AISI 1005 and 1070 steels, J. Mater. Sci. 27 (1992) 6777–6781.

[8] D. Psiachos, T. Hammerschmidt, R. Drautz, Ab initio study of the modification of elastic properties of α-iron by hydrostatic strain and by hydrogen interstitials, Acta Mater. 59 (2011) 4255–4263.

[9] P.W. Liu, J.K. Wu, Hydrogen susceptibility of an interstitial free steel, Mater. Lett. 57 (2003) 1224–1228.

[10] Y. Tsuchida, T. Watanabe, T. Kato, T. Seto, Effect of hydrogen absorption on strain-induced low-cycle fatigue of low carbon steel, Procedia Eng. 2 (2010) 555–561.

[11] V.R. Skal's'kyi, Z.T. Nazarchuk, S.I. Hirnyi, Effect of electrolytically absorbed hydrogen on Young's modulus of structural steel, Mater. Sci. 48 (2013) 491–499.

[12] P.B. Zhang, T.T. Zou, J.J. Zhao, P.F. Zheng, J.M. Chen, Diffusion and retention of hydrogen in vanadium in presence of Ti and Cr: first-principles investigations, J. Nucl. Mater. 484 (2017) 276–282.

[13] Paul S. Nnamchi, First principles studies on structural, elastic and electronic properties of new Ti-Mo-Nb-Zr alloys for biomedical applications, Mater. Des. 108 (2016) 60–67.

[14] H. Zhang, J.X. Deng, Z.W. Pan, Z.Y. Bai, L. Kong, J.Y. Wang, The tolerance of Ti_3SiC_2 to hydrogen-induced embrittlement: a first principles calculation, Mater. Lett. 166 (2017) 93–96.

[15] W.Q. He, H.B. Huang, X.Q. Ma, First-principles calculations on elastic and entropy properties in FeRh alloys, Mater. Lett. 195 (2017) 156–158.

[16] M. Tamer, Investigation of structural, electronic, elastic and optical properties of $Cd_{1-x-y}Zn_xHg_yTe$ alloys, AIP Adv. 6 (2016), 065115.

[17] Md. Afjalur Rahman, Md. Zahidur Rahaman, Md. Atikur Rahman, Thestructural, elastic, electronic and optical properties of MgCu under pressure: a first-principles study, Int. J. Mod. Phys. B 30 (2016), 1650199.

[18] P. Ravindran, Lars Fast, P.A. Korzhavyi, B. Johansson, J. Wills, O. Eriksson, Density functional theory for calculation of elastic properties of orthorhombic crystals: application to $TiSi_2$, J. Appl. Phys. 84 (9) (1998) 4891–4904.

[19] A.F. Chebanov, Determination of the temperature dependence of the bulk modulus of elasticity of certain pure metals, Mater. Sci. 27 (1992) 184–188.

[20] H.M. Ledbetter, R.P. Reed, Elastic properties of metals and alloys, I. Iron, nickel, and iron-nickel alloys, J. Phys. Chem. Ref. Data 2 (1973) 531–617.

[21] D.V. Edmonds, K. He, F.C. Rizzo, B.C. De Cooman, D.K. Matlock, J.G. Speer, Quenching and partitioning martensite—a novel steel heat treatment, Mater. Sci. Eng. A 438–440 (2006) 25–34.

[22] A.S. Kagan, A.G. Spektor, R.I. Tsil'man, Decomposition of martensite in steel ShKh15 in the process of quenching, Met. Sci. Heat Treat 23 (1981) 691–693.

[23] L.M. Kaputkina, V.G. Prokoshkina, Martensitic transformation and martensite structure in thermomechanically strengthened high-nitrogen steels, Mater. Sci. Eng. A 438–440 (2006) 228–232.

[24] P.C. Chen, P.G. Winchell, Martensite lattice changes during tempering, Metall. Trans. 11 (1980) 1333–1339.

[25] Robert J. Good, Theory of “cohesive” vs “adhesive” separation in an adhering system, J. Adhes. 4 (1972) 133–154.

[26] F. El Haj Hassan, H. Akbarzadeh, First-principles elastic and bonding properties of barium chalcogenides, Comput. Mater. Sci. 38 (2006) 362–368.